Available online at www.sciencedirect.com

ScienceDirect

IFAC Papers Online CONFERENCE PAPER ARCHIVE

IFAC PapersOnLine 53-2 (2020) 15306–15311

Optimal Control for Connected and Autonomous Vehicles at Signal-Free Intersections

Boli Chen * **Xiao Pan** ** **Simos A. Evangelou** ** **Stelios Timotheou** ***

* *Department of Electronic and Electrical Engineering at University College London, UK, (e-mail: boli.chen@ucl.ac.uk).*
** *Department of Electrical and Electronic Engineering, Imperial College London, UK, (e-mail: xiao.pan17@imperial.ac.uk, s.evangelou@imperial.ac.uk)*
*** *Department of Electrical and Computer Engineering and the KIOS Research and Innovation Center of Excellence, University of Cyprus, (e-mail: timotheou.stelios@ucy.ac.cy)*

Abstract: The development of connected and autonomous vehicles (CAVs) is one of the central aspects in the pathway towards future intelligent mobility systems. This paper addresses the problem of coordinating CAVs crossing an uncontrolled intersection so as to maintain safe and efficient traffic flow. The proposed control strategy is based on an optimal control framework that is formulated to minimize a weighted sum of total energy consumption and travel time of all CAVs by finding the optimal velocity trajectory of each vehicle. The design procedure starts with a proper formulation of the autonomous intersection crossing problem for CAVs, with various cases of energy recovery capability by the CAVs considered, to also investigate the influence of powertrain electrification on the intersection crossing problem. This yields an optimal control problem (OCP) with nonlinear and nonconvex dynamics and constraints. In order to ensure a rapid solution search and a unique global optimum, the OCP is reformulated via convex modeling techniques. Numerical results validate the effectiveness of the proposed approaches, while the trade-off between energy consumption and travel time is illustrated by Pareto optimal solutions.

Keywords: Connected and autonomous vehicles, Intersections crossing, Energy consumption, Optimization, Velocity control.

1. INTRODUCTION

The rapid advance of urbanization leads to overloaded urban roads and causes traffic congestion, which in turn increase overall energy use, emissions and travel time. The major bottleneck that leads to congestion is road intersections where flows of traffic merge from different directions. This has motivated growing research on traffic flow and vehicle motion control systems that can alleviate traffic congestion, especially at intersections. Traditionally, traffic lights are used to regulate flows that pass from an intersection to improve traffic capacity and safety without affecting the existing road infrastructure. Although a vast amount of literature exists that utilizes different methodologies for traffic light control, such as optimization (Fleck et al., 2015) and machine learning (Srinivasan et al., 2006), intersection crossing is still inefficient. More traffic signals usually come with higher cost and potentially increased rear-end vehicle collisions as drivers may abruptly stop at a yellow or a red light.

Due to the recent developments in information and communication technologies, such as vehicle-to-vehicle (V2V), and vehicle-to-infrastructure (V2X), the connected and autonomous vehicle (CAV) has been identified as a transformative technology that has a great potential to improve road traffic capacity and to reduce delays (Guanetti et al., 2018; Martinez et al., 2017). In this paper, the problem of autonomous intersection crossing is addressed, where multiple CAVs are optimally and cooperatively controlled to cross a signal-free intersection so as to minimize energy consumption subject to safety and throughput maximization requirements. The implications of this study are that vehicles can pass the intersection without a full stop, thereby both energy consumption and travel time can benefit from momentum conservation (Rios-Torres and Malikopoulos, 2016).

The research efforts that have been reported in the literature for coordinating CAVs at intersections can be categorized into centralized and decentralized approaches. The centralized schemes are regulated by a central controller that globally decides the trajectory for all CAVs. Huang et al. (2012); Zhang et al. (2015) propose the use of centralized approaches based on heuristic control rules that target safe and efficient scheduling of CAVs approaching the intersection. Although the rule-based methods are easy to implement and understand, they generally yield non-optimal control solutions. Some other centralized approaches have focused on numerical optimization algorithms, which guarantee global/local optimality and by which various control targets can be reached by a suitably

⋆ This work has been supported by the EPSRC Grant EP/N022262/1 and the European Unions Horizon 2020 research and innovation programme under grant agreement No 739551 (KIOS CoE), the Government of the Republic of Cyprus through the Directorate General for European Programmes, Coordination and Development and through the Research Promotion Foundation (Project: CULTURE/BR-NE/0517/14).

10.1016/j.ifacol.2020.12.2336

designed objective function, such as traffic throughput (Fayazi and Vahidi, 2018) and total travel time (Zohdy et al., 2012). Nonetheless, these approaches rely on non-convex optimization problems, which are computationally expensive, and therefore they are not applicable to a large number of vehicles. In the decentralized case, the motion of each CAV is determined by a local (to each vehicle) controller based on the information shared by other vehicles and the infrastructure (Colombo and Vecchio, 2014; Kim and Kumar, 2014). Recently, Malikopoulos et al. (2018) proposes a decentralized strategy for the co-optimization of energy consumption and travel time. The optimal solution is found analytically resorting to the Pontryagins Minimum Principle, thus it can be implemented online very efficiently. Although significant progress has been made, the available methods only utilize a highly simplified linear vehicle longitudinal model, in which the energy losses are neglected and the powertrain is conventional, while powertrain energy recovery is not addressed. Furthermore, the energy consumption (cost function) is approximated by the L^2-norm of the vehicle acceleration, which might not be realistic (Hadjigeorgiou and Timotheou, 2019).

This paper addresses the autonomous intersection crossing problem by a centralized methodology, where a weighted sum of the aggregate energy consumption and traveling time of all CAVs is optimized. The contributions of the present work are that in contrast with the available approaches: a) the vehicle dynamics in this work are modeled by a realistic longitudinal model that involves the air drag and rolling resistance losses, and the energy consumption is accurately formulated rather than utilizing the L^2-norm of the vehicle acceleration. b) the investigation is carried out for a wide range of powertrain energy recovery capability during braking (such an investigation for a single vehicle scenario is found in (Chen et al., 2019)) to characterize the impact of powertrain electrification on the optimal solution, c) the overall optimal control problem (OCP) is formulated as a convex optimization problem without substantial relaxation and approximation, and d) the resulting problem is solved by an OCP solver, GPOPS-II (Rao et al., 2010), with the Pareto optimal solutions generated to show the trade-off between energy consumption and travel time, and also the benefit of the convex formulation against the original non-convex OCP formulation in terms of energy and computation cost.

The rest of this paper is organized as follows. Section 2 introduces the intersection crossing problem for CAVs. The optimal control problem is formulated and convexified in Section 3. Numerical examples are illustrated in Section 4, followed by the concluding remarks in Section 5.

2. PROBLEM STATEMENT

A signal-free intersection is considered in the present work, as illustrated in Fig.1 (Malikopoulos et al., 2018; Rios-Torres and Malikopoulos, 2016). The center of the intersection is the *Merging Zone* (MZ), which is the area of potential lateral collision of vehicles. CAVs merging from each direction towards the MZ will first enter the *Control Zone* (CZ), in which the CAVs are coordinated by an *Intersection Controller* (IC). It is assumed that the IC can communicate without any error or delay with all CAVs that intend to cross the intersection, and then it determines the trajectory of all the CAVs to ensure the safe crossing of the MZ with an optimized objective in relation to the total energy consumption and travel time. In addition, the IC follows a First-In-First-Out (FIFO) control policy, whereby each vehicle must enter and leave

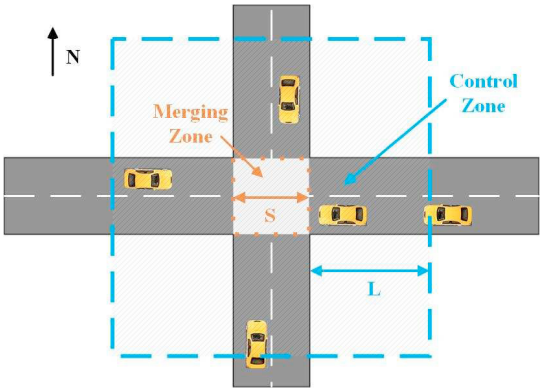

Fig. 1. Scheme of autonomous intersection crossing with connected and autonomous vehicles.

the MZ in the same order it entered the CZ. Without loss of generality, the MZ and CZ are considered to be squares of side S and $2L+S$, respectively, with $S<L$. As such, the distance from any CZ entry point to the entry of the MZ is L. For simplicity, it is also assumed that the roads only have two lanes and all the CAVs keep their initial directions throughout the CZ, such that lane changing and turns are not allowed in this study.

Let us denote N the total number of CAVs that will enter the CZ within a predefined time period T. All the CAVs are assumed identical, and the gross motion of a single CAV is described by the longitudinal dynamics:

$$\frac{d}{dt}v_i(t)=\frac{1}{m}(F_{w,i}(t)-F_r-F_{d,i}(t))\,,\quad i=1,2,\ldots,N, \tag{1}$$

where $v_i(t)$ is the velocity of the ith CAV, $m=1200\,\text{kg}$ is the vehicle mass, $F_r=f_r mg$ and $F_{d,i}(t)=f_d v_i^2(t)$ are the resistances of rolling and air drag, $f_r=0.01$ and $f_d=0.47$ are coefficients of rolling and air drag resistances, and $F_{w,i}$ is the powertrain driving or braking force acting on the wheels. The velocity and driving force of are constrained by permissible limits:

$$v_{\min}\le v_i(t)\le v_{\max}, \tag{2a}$$
$$F_{w,\min}\le F_{w,i}(t)\le F_{w,\max}, \tag{2b}$$

where $v_{\max}=15\,\text{m/s}$ and $v_{\min}=0.5\,\text{m/s}$ represent the maximum and minimum speed limits, prescribed by infrastructure requirements and traffic regulations (Hadjigeorgiou and Timotheou, 2019). Note that in order to satisfy the strict positivity requirement of the transformation in (3), the lower bound of the velocity is set to a small positive value. Moreover, the lower and upper limits of the driving force are determined respectively by $F_{w,\min}=ma_{\min}$ and $F_{w,\max}=ma_{\max}$ with $a_{\max}=2.5\,\text{m/s}^2$ the maximum (possible) acceleration of a CAV associated with the powertrain capability and $a_{\min}=-6.5\,\text{m/s}^2$ the maximum available deceleration during emergency braking subject to tire friction limits.

Since the traveled distance of each vehicle from the entry of the CZ to the exit of the MZ is fixed, it is reasonable to formulate and describe the problem in the space domain, in which the independent variable is traveled distance, s, instead of time. Moreover, in Section 3 it will be shown that the problem defined in the space domain can be formulated in a convex form. The transformation from time domain to space domain takes the following form, provided that the speed of the CAVs is strictly positive:

$$\frac{d}{ds}=\frac{1}{v_i}\frac{d}{dt}\,. \tag{3}$$

Then, the vehicle longitudinal dynamics are described by:

$$\frac{d}{ds}v_i(s) = \frac{F_{w,i}(s) - F_r - F_{d,i}(s)}{mv_i(s)},\ i = 1, 2, \ldots, N, \quad (4)$$

For $s \in [L, L+S]$, the following assumption is imposed:

Assumption 1. All CAVs enter the MZ at a same predefined speed $\bar{v} \in [v_{\min}, v_{\max}]$, and then maintain that speed inside the MZ, such that:

$$v_i(s) = \bar{v}\,,\ \ s \in [L, L+S]\,,\ \ \forall i \in \mathcal{N}, \quad (5)$$

where $\mathcal{N}$ is a set to designate the order in which the vehicles enter the CZ:

$$\mathcal{N} = \{1, 2, \ldots, N\} \in \mathbb{Z}^N. \quad (6)$$

As the model is formulated in the space domain, the individual travel time t_i of each CAV is introduced as a system state, with its state dynamics expressed by:

$$\frac{d}{ds}t_i(s) = \frac{1}{v_i(s)},\ \ i = 1, 2, \ldots, N. \quad (7)$$

The following assumption is imposed to validate the FIFO priority model:

Assumption 2. The entry times of all CAVs at the CZ are different, such that $t_i(0) \neq t_j(0)$, $i \neq j$.

Thus, $t_i(0) < t_j(0)$, $i < j$, $\forall i, j \in \mathcal{N}$. $\mathcal{N}$ can be further divided into two subsets as $\mathcal{N} = \mathcal{N}_p \cup \mathcal{N}_q$, where $\mathcal{N}_p \in \mathbb{Z}^{N_p}$ and $\mathcal{N}_q \in \mathbb{Z}^{N_q}$ collect the CAVs moving in longitudinal and lateral directions, respectively. With reference to (6), the FIFO control policy can be expressed as:

$$t_i(s) < t_j(s)\,,\ s \in \{L, L+S\}\,,\ i < j,\ \forall i, j \in \mathcal{N}. \quad (8)$$

Furthermore, for the safe crossing of all vehicles, lateral and rear-end collisions must be avoided at all times. A safe (minimum) separation gap is defined to avoid rear-end collision for CAVs traveling in the same direction. In contrast to the rear-end safety constraint deployed in (Malikopoulos et al., 2018) that enforces a constraint with a fixed safety (minimum) distance, the present work proposes the use of a more robust dynamic (velocity-dependent) minimum inter-vehicular distance, which represents more accurately the required gap. Since the problem is formulated in the space domain, it is convenient to introduce the gap as a time-gap for all $s \in [0, L]$ as follows:

$$t_i(s) - t_k(s) \geq T_\sigma + \frac{v_i(s)}{|a_{\min}|},\ k < i\,,\ \forall i, k \in \mathcal{N}, \quad (9)$$

where k denotes the index of the vehicle in front of the ith CAV in the same traveling direction, and $T_\sigma = 0.5$ is the response time of the vehicle braking system (Xie et al., 2019). The overall time-gap on the right hand side of (9) represents the minimum time that is required to stop the ith CAV if CAV k suddenly stops. As this separation gap is velocity dependent, it is less vulnerable to rear-end collisions that may be caused by velocity disturbances, in comparison to the fixed minimum distance applied in existing works (Hadjigeorgiou and Timotheou, 2019; Malikopoulos et al., 2018). Such an attribute may turn out to be very useful in practice as the actual velocity of the CAVs may be perturbed due to measurement noise, communication delays or even malicious attacks. Based on (5) (see Assumption 1), for $s \in [L, L+S]$ the path constraint (9) can be reduced to a single terminal constraint for each CAV as follows:

$$t_k(L) + T_\sigma + \frac{\bar{v}}{|a_{\min}|} \leq t_i(L)\,, \quad (10)$$

which prevents rear-end collisions inside the MZ.

On the other hand, the merging times of any two CAVs i and j from the perpendicular directions need to satisfy the constraint:

$$t_i(L) + \frac{S}{\bar{v}} \leq t_j(L)\,,\ \ i < j,\ \ i \in \mathcal{N}_p\,,\ j \in \mathcal{N}_q\,, \quad (11)$$

which ensures that vehicle j enters the MZ only after vehicle i has left the MZ. As it can be noticed, the FIFO control policy (8) is naturally guaranteed by (10) and (11). Finally, a further assumption is introduced to ensure that the initial states and control inputs are feasible:

Assumption 3. For any CAV i, none of the constraints (2) and (9) is active at $t_i(0)$.

The energy consumption of a CAV is evaluated by formulating the "wheel-to-distance" energy losses. A wide range of vehicle powertrain architectures is considered in the present study by defining the *energy recovery factor* $\rho \in [0, 1]$ as the ratio between regenerative braking power and the total braking power (Chen et al., 2019). Consequently, the energy dissipation function for a single CAV i is:

$$J_{e,i} = \int_0^{L+S} \begin{cases} F_{w,i}(s) & F_{w,i} \geq 0 \\ \rho F_{w,i}(s) & F_{w,i} < 0 \end{cases} ds\,. \quad (12)$$

As it can be noticed, different values of ρ allow different fractions of recuperation of the vehicle braking energy. In particular, the case $\rho = 0$ corresponds to a conventional vehicle (such as an internal combustion engine vehicle), while $\rho = 1$ indicates that all braking energy is recovered as in a highly hybridized or fully electric vehicle.

3. OPTIMAL CONTROL PROBLEM FORMULATION

This work aims to design an IC that optimizes the total energy consumption and travel time of all CAVs crossing the intersection subject to constraints related to physical limits and safety (as discussed in Section 2), by finding the optimal driving speed profile of each CAV. This section formulates the associated optimal control problem (OCP) with suitable approximations for convex reformulation.

The objective of the OCP is to find the wheel force, $F_{w,i}$, that minimizes a multi-objective function, expressed as follows:

$$J = \sum_{i=1}^{N} \left(W_1 \big(t_i(L) - t_i(0)\big) + W_2 \int_0^L \max(\rho F_{w,i}(s), F_{w,i}(s))\, ds \right) \quad (13)$$

where the second term is inferred from (12), and W_1 and W_2 are the weighting factors tuned to balance the trade-off between the total travel time and energy consumption, subject to constraints (2), (4), (7), (9), (10), and (11). Note that only the cost required to arrive at the MZ is considered since both the energy consumption and travel time within the MZ are fixed and independent of the optimal control strategy (see Assumption 1).

The dynamic model of the OCP, which describes the gross motion of all the CAVs, collects the differential equations (1) and (7), and therefore the dynamic order is $2N$. As it can be seen, the velocity dynamic equation (1) is nonlinear due to the air drag loss term. The nonlinearity can be conveniently removed, without introducing approximations, by transforming from the time domain to the space domain (see (4)), and performing the variable change $v_i(s) \to E_i(s)$, where $E_i(s)$ is the kinetic energy of CAV i (Uebel et al., 2019), defined by: $E_i(s) = \frac{1}{2}mv_i^2(s)$. The system dynamic equations (4) and (7) can then be rewritten as:

$$\frac{d}{ds}E_i(s) = F_{t,i}(s) + F_{b,i}(s) - F_r - 2\frac{f_d}{m}E_i(s)\,, \quad (14a)$$

$$\frac{d}{ds}t_i(s) = \frac{1}{\sqrt{2E_i(s)/m}}, \quad i \in \mathcal{N}, \quad (14b)$$

where the first equation is linear, and the wheel force $F_{w,i}(s)$ is broken down to two separate control inputs, the traction force $F_{t,i}(s) \geq 0$ and braking force $F_{b,i}(s) < 0$. As such, the energy consumption $\int_0^L \max(\rho F_{w,i}, F_{w,i})\, ds$ in (13) can be expressed as a linear function of the two control inputs, $F_{t,i}(s)$ and $F_{b,i}(s)$. It is clear from (2b) that the two inputs are constrained by:

$$F_{w,\min} \leq F_{b,i}(s) \leq 0, \quad 0 \leq F_{t,i}(s) \leq F_{w,\max}. \quad (15)$$

Another important step to convexify the nonlinear OCP is to linearize the nonlinear dynamics of $t(s)$ in (14b), and to do so let us introduce a new control variable $\zeta(s)$:

$$\frac{d}{ds}t_i(s) = \zeta_i(s)\,, \quad (16a)$$

$$\zeta_i(s) \geq \frac{1}{\sqrt{2E_i(s)/m}}, \quad i \in \mathcal{N}. \quad (16b)$$

Thus, the nonlinearity in the differential equation (14b) is removed and replaced by a convex path constraint (16b), with the equality condition precisely achieved at all times, since minimization of the total travel time (see (13)) also minimizes $\zeta_i(s)$.

In view of the speed limits (2a), the state of kinetic energy $E_i(s)$ is bounded by:

$$E_{\min} \leq E_i(s) \leq E_{\max},\ i \in \mathcal{N}, \quad (17)$$

where $E_{\min} = \frac{1}{2}mv_{\min}^2$ and $E_{\max} = \frac{1}{2}mv_{\max}^2$ are respectively determined by the minimum velocity $v_{\min}$ and maximum velocity $v_{\max}$ for the intersection crossing.

After replacing $v_i(s)$ with $E_i(s)$, the safety constraints (10) and (11) remain linear, whereas (9) becomes:

$$t_i(s) - t_k(s) \geq T_\sigma + \frac{\sqrt{2E_i(s)/m}}{|a_{\min}|}, \ s \in [0, L]\,, \quad (18)$$

which is non-convex. It is possible to turn this back into a convex condition by approximating the nonlinear relationship between kinetic energy and velocity, $v_i(s) = \sqrt{2E_i(s)/m}$, by a linear function of E_i:

$$f(E_i(s)) = a_0 + a_1 E_i(s), \quad \forall E_i(s) \in [E_{\min}, E_{\max}]\,, \quad (19)$$

where a_0 and a_1 are obtained by linear regression to fit the line tangentially to the original curve, as shown in Fig. 2. Since by virtue of the tangential linear fit

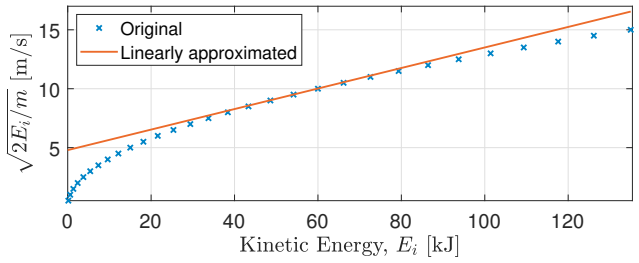

Fig. 2. Linearly approximated relationship between kinetic energy and velocity, where the points (×) of the nonlinear relationship are linearly spaced in velocity.

$f(E_i(s)) \geq \sqrt{2E_i(s)/m}$ at any s, a solution to the control problem obtained by solving the approximated problem is conservative and always feasible for the original problem.

By defining the state and control vectors:
$\mathbf{x} = [E_1, E_2, \ldots, E_N, t_1, t_2, \ldots, t_N]$,
$\mathbf{u} = [F_{t,1}, F_{t,2}, \ldots, F_{t,N}, F_{b,1}, F_{b,2}, \ldots, F_{b,N}, \zeta_1, \zeta_2, \ldots, \zeta_N]$,
the OCP for autonomous intersection crossing is formulated as follows:

$$\min_{\boldsymbol{u}} \ J \quad (20a)$$

$$\textbf{s.t.:} \quad \frac{d}{ds}\boldsymbol{x}(s) = f(\boldsymbol{x}(s), \boldsymbol{u}(s))\,, \quad (20b)$$

$$\Psi(\boldsymbol{x}(s), \boldsymbol{u}(s)) \leq 0\,, \quad (20c)$$

$$\boldsymbol{b}(\boldsymbol{x}(0), \boldsymbol{x}(L)) = 0\,, \quad (20d)$$

where:

$$J = \sum_{i=1}^{N}\left(W_1\int_0^L \zeta_i(s)\, ds + W_2\int_0^L F_{t,i}(s) + \rho F_{b,i}(s)\, ds\right). \quad (21)$$

The dynamic constraints (20b) are formed by two sets of linear differential equations (14a) and (16a), which have identical form for all CAVs. Inequality constraints (20c) comprise the path constraints for physical limits and driving safety, including (10), (11),(15), (16b), (17) and,

$$t_i(s) - t_k(s) \geq T_\sigma + \frac{a_0 + a_1 E_i(s)}{|a_{\min}|}\,, s \in [0, L] \quad (22)$$

obtained from (18) and (19). The boundary conditions (20d) specify the initial and terminal conditions of the states. As mentioned previously, the initial conditions $\boldsymbol{x}(0)$ are randomly generated while fulfilling the conditions imposed in Assumption 3. Finally, the OCP problem is completed by the following terminal condition to meet Assumption 1:

$$E_i(L) = \frac{1}{2}m\bar{v}^2\,, \ \ i \in \mathcal{N}. \quad (23)$$

4. NUMERICAL RESULTS

The evaluation of the proposed strategy is performed in a case study in two steps: 1) the proposed convex OCP (see (20)) is solved for CAVs with different levels of energy recovery capability determined by ρ, to investigate and compare the impact of ρ on the optimum of the weighted sum of energy consumption and travel time; 2) the conservativeness of the convex relaxation is investigated by comparing the solution of the convex OCP with the solution solved by the original more accurate non-convex OCP (see (20) but with (14b) used instead of (16) and (18) used instead of (22)).

In the present case study, an intersection with $S = 10\,\text{m}$ and $L = 150\,\text{m}$ is considered. The constant velocity inside the MZ is set to $\bar{v} = 10\text{m/s}$. The arrival speed $v_i(0)$, time $t_i(0)$ and direction of each CAV are randomly generated as presented in (Hadjigeorgiou and Timotheou, 2019). Without loss of generality, it is assumed that the $v_i(0)$, $i \in \mathcal{N}$ follow a uniform probability distribution between $v_{\min}$ and $v_{\max}$, while the directions are also subject to a uniform distribution. Arrival times are modeled using Poisson processes under the constraints of Assumptions 2 and 3. As shown in Fig. 1, there is no interaction between vehicles traveling in opposite directions. Therefore, in order to make the presentation of the results clearer, it is reasonably assumed that there is only one lane in each perpendicular road and all the CAVs travel in the same direction in each lane. A total number of 20 CAVs is considered, with 12 randomly selected vehicles traveling in the north-south direction and 8 vehicles in the east-west direction. Additionally, the arrival speed of

one of the vehicles traveling in the north-south direction is substituted with a value close to the upper speed limit, and the arrival speed of a vehicle traveling in the east-west direction is substituted with a value close to the lower speed limit, to enable a more exhaustive investigation. All the OCPs are solved in the Matlab environment by GPOPS-II software.

The optimal solutions of the convex OCP are reported in Figs. 3 to 5(a). To compare the optimal solutions for different ρ, at first the weights of the objective function are set to $W_1 = W_2 = 1$ and solutions for $\rho = 0$ and $\rho = 1$ are found.

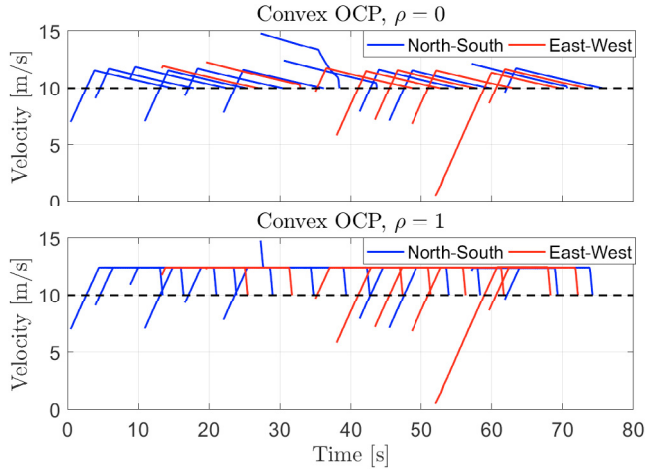

Fig. 3. Optimal driving speed profiles of CAVs by solving the convex OCP with $\rho = 0$ (top) and $\rho = 1$ (bottom). The dash lines denote the constant velocity $\bar{v}$ inside the MZ.

As it can be seen in Fig. 3, the optimal speed profiles in both scenarios behave very differently. When $\rho = 0$, the optimal driving speeds of all the CAVs follow the pulse and glide (PnG) strategy that is mainly formed by initially rapid acceleration to a maximum velocity followed by a period of coasting and in some cases intensive braking at the end of the maneuver to satisfy the terminal condition (23). Depending on the initial speed, the behavior of each CAV may start from any PnG stage. For example, if the CAV enters the CZ at a high velocity, instead of initially accelerating the CAV, the IC controller enforces the CAV to glide down immediately in order to reach the desired velocity $\bar{v}$ at the end. More braking is preferred when $\rho = 1$ as compared to the case with $\rho = 0$ as the braking energy can be recuperated for future use. The optimal solutions for $\rho = 1$ further suggest all CAVs accelerate to a cruise speed value and maintain this speed until they approach the MZ. Note that all the CAVs cruise at the same velocity (of 12.42m/s), which naturally avoids rear-end collisions according to the imposed constraints. Furthermore, the individual CAV optimal speed profile results as ρ varies are compatible with results obtained in previous single-vehicles studies (Chen et al., 2018). For example, as compared to the PnG solution for $\rho = 0$, for $\rho = 1$ the constant cruise speed is a solution that allows to reduce the initial peak speed (to avoid excessive air drag losses) and maximize energy recovery at the end of the maneuver, to improve the energy efficiency without compromising the travel time.

In order to verify that the FIFO policy and safety constraints are followed during the simulations, the traveled distance of each CAV is plotted against time in Fig. 4 for both $\rho = 0$ and $\rho = 1$ cases. It can be observed that all the CAVs pass the intersection in sequence without

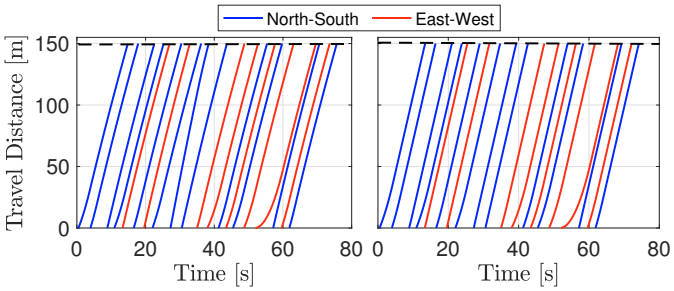

Fig. 4. Traveled distance trajectories of CAVs when following optimal driving speeds by solving the convex OCP with $\rho = 0$ (left) and $\rho = 1$ (right). The black lines denote the vehicles entry the MZ

rear-end and lateral collisions (none of the trajectories intersect). Moreover, any two vehicles traveling in the same direction satisfy the safety minimum time-separation (see (22)), while the distance of two vehicles traveling in perpendicular directions may be very close to each other as they only need to avoid the lateral collision in the MZ (see (11)). Finally, by further analysis of the results it is found that the constraints (9), (10), and (11) are satisfied in the solutions of the convex OCP, which justifies the convex relaxation (see (22)) and shows the validity of the solution for the original problem.

To show the trade-off between the total travel time and the energy consumption, Pareto solutions in both scenarios of ρ values are investigated by a thorough tuning of the weights W_1 and W_2 under the same initial conditions of vehicles speed, direction and arrival time. As it can be seen

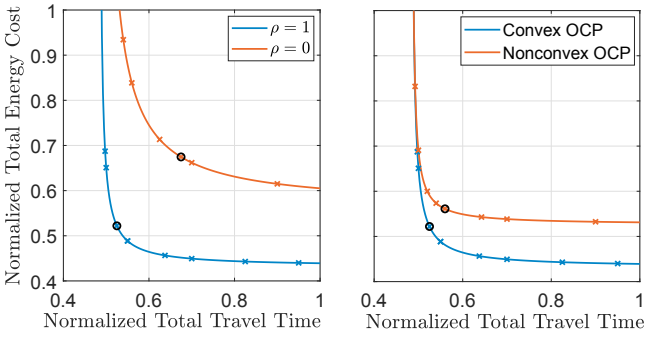

Fig. 5. Left (a): Pareto fronts of the convex OCP for $\rho = 0$ and $\rho = 1$. Right (b): Pareto fronts of the convex OCP and non-convex OCP for $\rho = 1$. (The min-max solutions are highlighted by $\circ$, and both the total energy cost and total travel time are normalized against their maximum value solutions of (400 s, 1000 kJ)).

in Fig. 5(a), the Pareto front for $\rho = 0$ is always above the Pareto front for $\rho = 1$ since the energy recovery enables a significant energy saving. In particular, to achieve the total travel time of 250 s (0.625 when normalized), the powertrain case with full regenerative braking capability ($\rho = 1$) can approximately save roughly 35% energy as compared to the conventional powertrain case ($\rho = 0$). Moreover, the results for $\rho = 1$ indicate that the min-max Pareto solution is obtained at normalized values of $(0.525, 0.525)$, which are equivalent to (210 s, 525 kJ), while an increase in travel time of 20% from the Pareto solution leads to an approximated 13% reduction in energy consumption. For any solutions further away from the Pareto solution, it can be observed that both energy consumption and travel time are extremely sensitive to the

changes of each other. In the case of $\rho = 0$, the min-max Pareto solution is at $(270\,\text{s}, 675\,\text{kJ})$. Increasing the travel time from the Pareto solution by 20% can save about 7% energy usage, while further increase in travel time can lead to up to 10.3% energy consumption reduction. Thus, when the CAVs have conventional powertrains, both energy and travel time consumption are less sensitive to the changes of each other as compared to the case of $\rho = 1$.

To gain more insight into the optimality of the proposed convex optimization method, the next example with $\rho = 1$ is carried out to explicitly compare the solution of the convex OCP and the solution of the original non-convex OCP. In Fig. 5(b), the Pareto fronts of both convex and non-convex OCPs are shown for the same initial conditions as used previously and shown in Fig. 3. As it can be noticed, the solution of the convex OCP is equally and in some cases more optimal than the solution of the non-convex OCP, which highlights the benefit of the convex relaxation. As an example, at a total travel time of 250 s the convex optimization solution is about 15% better than the solution of the non-convex original OCP in terms of energy economy. To further emphasize the improvement of the convex OCP on the computational efficiency, the average running time of both OCP cases are compared. The convex OCPs approximately consume one fifth of the time requested by the non-convex OCPs. On the other hand, the equality of the convex and non-convex OCP solutions holds when the total travel time is small. This can be understood that each CAV has to travel at least for a portion of its trajectory at its maximum speed to achieve the desired travel time, thus yielding the same or very similar solution for both OCPs. When the travel time is relaxed, there is more room for optimization, and therefore the non-convex OCP may reach local optimal solutions, which are less optimal than the single and well approximated 'global optimum' solution by the convex optimization.

5. CONCLUSIONS

This paper proposes a novel centralized control strategy for controlling CAVs to cross a signal-free intersection. Both travel time and energy consumption is optimized by finding the optimal velocity trajectory of each vehicle subject to vehicle operational and intersection safety constraints. The overall control problem is formulated by utilizing convex modeling techniques, yielding a convex optimal control problem (OCP). The numerical examples investigate the trade-off between travel time and energy consumption for different powertrain systems, characterized by the energy recovery factor. Moreover, the conservativeness and the optimality of the convex OCP formulation are verified by comparing the convex solutions with the solutions from the original non-convex problem. Future research will investigate practical uncertainties, such as noisy measurements, communication delays, and more realistic priority models rather than the First-In-First-Out policy.

REFERENCES

Chen, B., Evangelou, S., and Lot, R. (2019). Series hybrid electric vehicle simultaneous energy management and driving speed optimization. *IEEE/ASME Transactions on Mechatronics*, 24(6), 2756 – 2767.

Chen, B., Evangelou, S.A., and Lot, R. (2018). Fuel efficiency optimization methodologies for series hybrid electric vehicles. In *2018 IEEE Vehicle Power and Propulsion Conference (VPPC)*, 1–6. IEEE.

Colombo, A. and Vecchio, D.D. (2014). Least restrictive supervisors for intersection collision avoidance: A scheduling approach. *IEEE Transactions on Automatic Control*, 60(6), 1515–1527.

Fayazi, S.A. and Vahidi, A. (2018). Mixed-integer linear programming for optimal scheduling of autonomous vehicle intersection crossing. *IEEE Transactions on Intelligent Vehicles*, 3(3), 287–299.

Fleck, J.L., Cassandras, C.G., and Geng, Y. (2015). Adaptive quasi-dynamic traffic light control. *IEEE Transactions on Control Systems Technology*, 24(3), 830–842.

Guanetti, J., Kim, Y., and Borrelli, F. (2018). Control of connected and automated vehicles: State of the art and future challenges. *Annual reviews in control*, 45, 18–40.

Hadjigeorgiou, A. and Timotheou, S. (2019). Optimizing the trade-off between fuel consumption and travel time in an unsignalized autonomous intersection crossing. In *Proceedings of the 2019 IEEE Intelligent Transportation Systems Conference (ITSC), Auckland, NZ, October 27-30, 2019*, 2443–2448. IEEE.

Huang, S., Sadek, A.W., and Zhao, Y. (2012). Assessing the mobility and environmental benefits of reservation-based intelligent intersections using an integrated simulator. *IEEE Transactions on Intelligent Transportation Systems*, 13(3), 1201–1214.

Kim, K.D. and Kumar, P.R. (2014). An mpc-based approach to provable system-wide safety and liveness of autonomous ground traffic. *IEEE Transactions on Automatic Control*, 59(12), 3341–3356.

Malikopoulos, A.A., Cassandras, C.G., and Zhang, Y.J. (2018). A decentralized energy-optimal control framework for connected automated vehicles at signal-free intersections. *Automatica*, 93, 244–256.

Martinez, C.M., Hu, X., Cao, D., Velenis, E., Gao, B., and Wellers, M. (2017). Energy management in plug-in hybrid electric vehicles: Recent progress and a connected vehicles perspective. *IEEE Transactions on Vehicular Technology*, 66(6), 4534–4549.

Rao, A.V., Benson, D., Darby, C., Patterson, M., Francolin, C., Sanders, I., and Huntington, G. (2010). Gpops: A matlab software for solving multiple-phase optimal control problems using the gauss pseudospectral method. *ACM Transactions on Mathematical Software*, 37(2).

Rios-Torres, J. and Malikopoulos, A.A. (2016). A survey on the coordination of connected and automated vehicles at intersections and merging at highway on-ramps. *IEEE Transactions on Intelligent Transportation Systems*, 18(5), 1066–1077.

Srinivasan, D., Choy, M.C., and Cheu, R.L. (2006). Neural networks for real-time traffic signal control. *IEEE Transactions on intelligent transportation systems*, 7(3), 261–272.

Uebel, S., Murgovski, N., Bäker, B., and Sjöberg, J. (2019). A two-level mpc for energy management including velocity control of hybrid electric vehicles. *IEEE Transactions on Vehicular Technology*, 68(6), 5494–5505.

Xie, S., Hu, X., Liu, T., Qi, S., Lang, K., and Li, H. (2019). Predictive vehicle-following power management for plug-in hybrid electric vehicles. *Energy*, 166, 701–714.

Zhang, K., Zhang, D., de La Fortelle, A., Wu, X., and Gregoire, J. (2015). State-driven priority scheduling mechanisms for driverless vehicles approaching intersections. *IEEE Transactions on Intelligent Transportation Systems*, 16(5), 2487–2500.

Zohdy, I.H., Kamalanathsharma, R.K., and Rakha, H. (2012). Intersection management for autonomous vehicles using icacc. In *2012 15th international IEEE conference on intelligent transportation systems*, 1109–1114. IEEE.